This article has been accepted for publication in a future issue of this journal, but has not been fully edited. Content may change prior to final publication. Citation information: DOI 10.1109/JESTPE.2020.2967508, IEEE Journal of Emerging and Selected Topics in Power Electronics

Position Estimation Deviation Suppression Technology of PMSM Combining Phase Self-compensation SMO and Feed-forward PLL

Gang Liu, Haifeng Zhang, Xinda Song

***Abstract*—The sensorless drive method of the permanent magnet synchronous motor (PMSM) has attracted wide attention for its low cost and high reliability. As a critical technology, a fast and high-precision rotor position estimation is essential. This work addresses the position estimation deviation issue of the sensorless drive method based on the sliding mode observer (SMO) and phase-locked loop (PLL). A non-linear equivalent model of the SMO is established to analyze and compensate for the position estimation deviation caused by the SMO, and a feed-forward PLL is employed to suppress the steady-state position tracking error under variable speed operation. Firstly, the phase-frequency characteristic of the SMO is obtained by studying the SMO and the switching functions in detail. Then, the analysis of the conventional PLL is carried out in terms of the error transfer function. Besides, the position estimation performance of the feed-forward PLL is discussed with the dynamic error coefficient method. Theoretical analysis and experimental evaluation validated the effectiveness of the proposed position estimation deviation suppression technology of the PMSM combining the phase self-compensation SMO and the feed-forward PLL.**

***Index Terms*—sensorless drive, position estimation, sliding mode observer (SMO), non-linear model, phase locked loop (PLL), permanent magnet synchronous motor (PMSM)**

I. Introduction

COMPARING with the direct current motor and induction motor, the permanent magnet synchronous motor (PMSM) has the advantages of simple structure, high power density, high energy efficiency and reliable operation. With the reduction of the cost of permanent magnet materials and the development of control technology, the PMSM has been widely used in a variety of applications [1–3].

It is well known that the rotor position information is essential for the control of the PMSM. It can be obtained by mechanical position sensors or estimated through the phase voltages and currents [4, 5]. Even though the mechanical position sensors can work from standstill to the high speed, it increases the complexity of the mechanical structure and increases costs [6, 7]. Especially, mechanical position sensors would be damaged in humid, high-vibration and dusty industrial environments. Therefore, the sensorless drive of the PMSM has attracted extensive interest because of its space-saving, high reliability and low cost.

In middle and high speed ranges, methods based on the fundamental back EMF observers, such as flux observers, full/reduced-order state observers, model reference adaptive systems (MRASs), extended Kalman filters (EKFs), and sliding mode observers (SMOs) are extensively applied to the rotor position estimation. They are proposed to solve different types of problems, and they also have different application limitations. The flux observer has quite a simple structure with a fast dynamic response. However, due to its pure integral operation, the DC biases of the current and voltage measurements, as well as the initial condition, would affect the rotor position estimation accuracy [8, 9]. Full/reduced-order state observers are important methods employed in the rotor position estimation. They can achieve fast position estimation with a high-reliability but is sensitive to the parameter variations [10, 11]. MRASs can achieve a quite high position estimation accuracy if the model and parameters are accurate enough [8, 12, 13]. In a noisy environment, the EKF can work well and give a recursive optimum position estimation [14, 15]. However, the complex matrix operations aggravate the computational burden of the control system, which limits the applications in the high-speed range [16]. The SMO has emerged as an interesting candidate to estimate the rotor position for its simple structure, high robustness, and low sensitivity to the parameter variations [17–20].

The position estimation method combining the SMO and the phase-locked loop (PLL) is a commonly used in industrial applications, where the SMO is used to estimate the back electromotive force (EMF) and the PLL is adopted to track the rotor position with the estimated back EMF. Numerous studies were presented to improve the rotor position estimation accuracy based on the SMO and the PLL. One concerns the chattering suppression of the SMO, and the other concerns the reduction of the harmonic position error. To deal with the chattering, in [13], the sigmoid function is introduced to replace the sign function, and the sliding mode gain is adjusted through the fuzzy control algorithm. In [21], a second-order SMO with the super-twisting algorithm was presented for the rotor position and speed estimation, which can dramatically alleviate chattering behavior. Among these, adopting the sigmoid function as the switching function is a feasible and effective method to reduce the chattering [22–24]. In order to improve the harmonic suppression ability, in [25], a normalization of the equivalent back EMF for the PLL tracking estimator was

This work was supported in part by the National Natural Science Foundation of China (61773041), and in part by the Foundation for Innovative Research Groups of the National Natural Science Foundation of China (61721091).

Gang Liu, Haifeng Zhang and Xinda Song are with the School of Instrumentation and Optoelectronic Engineering, the Beijing Engineering Research Center of High-Speed Magnetically Suspended Motor Technology and Application, and also with Ningbo Innovation Research Institute, Beihang University, Beijing 100191, China (e-mail:lgang@buaa.edu.com, jackzhang-haifeng@126.com, songxinda@buaa.edu.cn).

proposed to improve the rotor position estimation accuracy. In [7], an orthogonal PLL with two synchronous frequency extract filters that were used to extract the fundamental wave of the back EMF was proposed, and the proposed method can effectively reduce the back EMF harmonic error.

The position estimation error is comprised of a position deviation and harmonic position error. As reviewed previous, the harmonic position error has been greatly improved, but the position estimation deviation issues do not obtain enough concerns. As presented in [26], the position estimation deviation is mainly caused by the parameter uncertainties, and parameter identification technologies are required to diminish the deviation. In [21], a parallel adaptive identification method of stator resistance is designed relying on derivatives of rotor flux and stator current to improve the near-zero speed operation performance of sensorless induction motor drives. In [15], the resistance uncertainties caused by temperature variation were taken into account with an online resistance observer, which improved position estimation accuracy and the robustness of the STA-SMO. However, they did not consider the effect of the observer on the accuracy of the position estimation. In [27], it is reported that when the estimated value is a persistent excitation, a time delay between the actual value and its estimation may appear due to the non-zero phase response of the observer. A very high gain can reduce the delay to a low level [28]. However, it is not always effective since it may introduce excessive noise to harm the stability of the observer. Another way is trying to estimate the time delay. In [29], a current control method of a six-phase induction machine drive based on the sliding mode was proposed and the time delay estimation technology was used to reconstruct the unmeasurable status. In [30], authors combined the time delay estimation method and the sliding mode to allow the stator current to the reference in finite time.

It is observed in practice that when the sigmoid function replaces the sign function, a serious position estimation deviation relating to the speed appears. To reduce the position estimation deviation, as analyzed above, increasing the sliding mode gain or adopting the time delay estimation technology may be useful. However, increasing the sliding mode gain would make the chattering more severe, and the time delay estimation technology may face the problem of limited estimation accuracy and complicated implementation process. Contrary to the two methods, this paper proposes a non-linear equivalent model of the SMO to analyze and compensate for the deviation.

Variable speed motors, such as reaction flywheels, blowers, compressors and pumps, are commonly used in industrial applications. They need to perform acceleration and deceleration operations frequently. However, as a typical type-II system, the conventional PLL is not fast enough to track the rotor position in acceleration and deceleration operations with zero steady-state position tracking error [8, 31, 32]. If a sudden speed change occurs, the position estimation error would dramatically increase and even cause tracking failure. It suggested introducing the speed to the PLL to improve the position tracking speed cite abdelrahem2017finite, preindl2010sensorless, bierhoff2017general, but it did not give sufficient design details and theoretical analysis. In practice, it may be not feasible to feed the speed directly to the PLL, because it dramatically increases the bandwidth of the PLL. Therefore, this paper gives design details of the feed-forward PLL with a low pass filter and the analysis of the effect of the feed-forward path on the PLL in theory. It is helpful for the parameter design of the feed-forward PLL in engineering.

The main contribution of this paper is to solve the position estimation deviation problem in the sensorless drive based on the SMO and PLL. A phase self-compensation method of the SMO is proposed by establishing a non-linear equivalent model, which can compensate for the rotor position deviation caused by the phase lag of the SMO. The proposed feed-forward PLL can suppress the steady-state estimation deviation under acceleration and deceleration operations, and it is also of benefit to reducing the harmonic position error.

II. Sensorless Drive Method of PMSM Based on SMO and PLL

The diagram of the sensorless drive method of the PMSM based on the SMO and PLL is shown in Fig. 1, where the SMO is used to reconstruct the back EMF with the phase voltages and currents, and the PLL is adopted to track the rotor position.

A. Mathematical Model of PMSM

The mathematical model of the PMSM in α-β reference frame is given by

$$\begin{cases} u_\alpha = Ri_\alpha + L\dfrac{di_\alpha}{dt} + e_\alpha \\ u_\beta = Ri_\beta + L\dfrac{di_\beta}{dt} + e_\beta \end{cases} \tag{1}$$

where $u_{\alpha,\beta}$, $i_{\alpha,\beta}$ and $e_{\alpha,\beta}$ represent the terminal voltages, phase currents and back EMFs in α-β axis, respectively; R, L are the resistance and inductance of the stator winding. The back EMFs are

$$\begin{cases} e_\alpha = -\psi_f\omega_e \sin(\theta_e) \\ e_\beta = \psi_f\omega_e \cos(\theta_e) \end{cases} \tag{2}$$

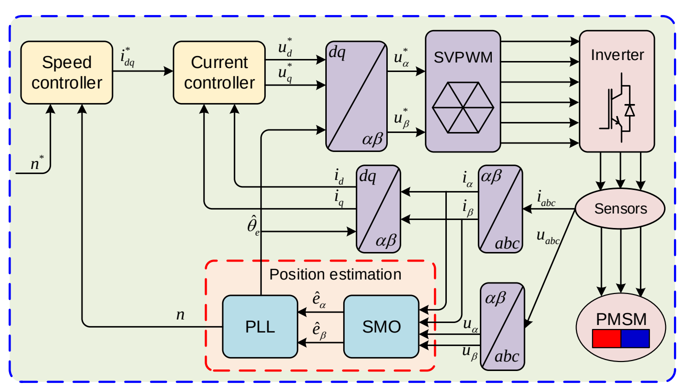

Fig. 1. Diagram of the conventional sensorless drive method of the PMSM based on SMO and PLL.

where θ_e is the rotor electrical position; ω_e is the electrical angular velocity; ψ_f is the permanent magnet flux linkage. From (2), ω_e can be obtained as

$$\omega_e = \frac{1}{\psi_f}\sqrt{\left(e_\alpha^2 + e_\beta^2\right)} \tag{3}$$

B. Design of SMO

Considering the phase currents as the state variables, the PMSM model (1) is rewritten as

$$\begin{cases} \dot{i}_\alpha = \dfrac{u_\alpha - Ri_\alpha - e_\alpha - \xi_\alpha}{L} \\ \dot{i}_\beta = \dfrac{u_\beta - Ri_\beta - e_\beta - \xi_\beta}{L} \end{cases} \tag{4}$$

where $\xi_{\alpha,\beta}$ are the equivalent errors of the model uncertainties, measurement errors, and external disturbances.

Based on (4), a SMO is designed as

$$\begin{cases} \dot{\hat{i}}_\alpha = \dfrac{u_\alpha - R\hat{i}_\alpha - v_\alpha}{L}, v_\alpha = k_s f(\tilde{i}_\alpha) \\ \dot{\hat{i}}_\beta = \dfrac{u_\beta - R\hat{i}_\beta - v_\beta}{L}, v_\beta = k_s f(\tilde{i}_\beta) \end{cases} \tag{5}$$

where the symbol ˆ represents the estimated values of the relevant variables; $f(x)$ is the switching function; $\tilde{i}_{\alpha,\beta} = \hat{i}_{\alpha,\beta} - i_{\alpha,\beta}$; k_s is the sliding mode gain.

Subtracting (4) from (5) yields the error dynamic of the currents as

$$\begin{cases} \dot{\tilde{i}}_\alpha = \dfrac{-R\tilde{i}_\alpha + e_\alpha + \xi_\alpha - v_\alpha}{L} \\ \dot{\tilde{i}}_\beta = \dfrac{-R\tilde{i}_\beta + e_\alpha + \xi_\beta - v_\beta}{L} \end{cases} \tag{6}$$

According to the variable structure theory, a sliding surface is designed as

$$S = \begin{bmatrix} \tilde{i}_\alpha \\ \tilde{i}_\beta \end{bmatrix} = 0 \tag{7}$$

The stability analysis of the SMO is given by using a Lyapunov function

$$V = \frac{1}{2}S^T S > 0 \tag{8}$$

If the time derivative of the Lyapunov function

$$\dot{V} = V_1 + V_2 + V_3 \tag{9}$$

is negative definite, the sliding mode will be enforced after a finite time interval, where

$$V_1 = -\frac{R}{L}\left[\tilde{i}_\alpha^2 + \tilde{i}_\beta^2\right],$$

$$V_2 = \frac{1}{L}\left[\tilde{i}_\alpha\left(e_\alpha + \xi_\alpha\right) - k_s\tilde{i}_\alpha f(\tilde{i}_\alpha)\right],$$

and

$$V_3 = \frac{1}{L}\left[\tilde{i}_\beta\left(e_\beta + \xi_\beta\right) - k_s\tilde{i}_\beta f(\tilde{i}_\beta)\right].$$

It is clear from (9) that $V_1 < 0$, and if $V_2 < 0$, the occurrence of sliding mode can be achieved. Thus, the sliding mode gain k_s can be selected as

$$k_s > \max\left(|e_\alpha| + |\xi_\alpha|, |e_\beta| + |\xi_\beta|\right) \tag{10}$$

When the system reaches the sliding surface, $S = \dot{S} = 0$. Based on the equivalent principle of the SMO, the estimated back EMFs are

$$\begin{cases} \hat{e}_\alpha = \dfrac{\omega_s}{s + \omega_s} v_\alpha \\ \hat{e}_\beta = \dfrac{\omega_s}{s + \omega_s} v_\beta \end{cases} \tag{11}$$

where $\hat{e}_{\alpha,\beta}$ are the estimated back EMFs, and the low-pass filter $\frac{\omega_s}{s+\omega_s}$ in (11) is used to filter the high-frequency components of the SMO's output. After the estimated back EMFs are obtained, a PLL, as shown in Fig. 2, is adopted to track the rotor position. It can be seen that the PLL is a second-order system that contains a phase detector (PD), a loop filter (LF) and a voltage-controlled oscillator (VCO). In this study, a proportional-integral (PI) controller is used as the loop filter.

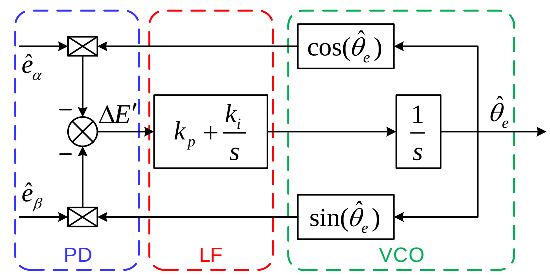

Fig. 2. Diagram of the conventional PLL in α-β reference frame.

III. Phase Self-compensation SMO And Feed-forward PLL

A. Phase Self-compensation Method of SMO

The sign and sigmoid functions are the commonly used switching functions, and the sigmoid function shows better performance to suppress the chattering. However, it is observed in real applications that when the sigmoid function replaces the sign function, it would exist a position estimation deviation. In this section, the reason for the deviation is studied in detail by establishing a non-linear equivalent model of the SMO.

The equivalent gains of the sign and sigmoid functions are

$$\begin{cases} k_{fn} = \left|\dfrac{1}{x}\right|, f(x) = \text{sign}(x) \\ k_{fd} = \dfrac{1 - e^{-x}}{x(1 + e^{-x})}, f(x) = \text{sigmoid}(x) \end{cases} \tag{12}$$

where x is the input variable of the function; k_{fn} and k_{fd} are the equivalent gains of the sign and sigmoid functions, respectively. It is noted that an upper limit of the equivalent gain of the sign function is set to avoid calculation crashes since it tends to be infinite at $x = 0$.

Based on (5) and (6), the diagram of the non-linear equivalent model of the SMO is obtained in Fig. 3, where k_f is the equivalent gain of the switching function. It can be seen from Fig. 3 that the SMO is a variable gain control system since the equivalent gain of the switching function is non-constant. The closed-loop transfer function of the non-linear equivalent model at a certain k_f is

This article has been accepted for publication in a future issue of this journal, but has not been fully edited. Content may change prior to final publication. Citation information: DOI 10.1109/JESTPE.2020.2967508, IEEE Journal of Emerging and Selected Topics in Power Electronics

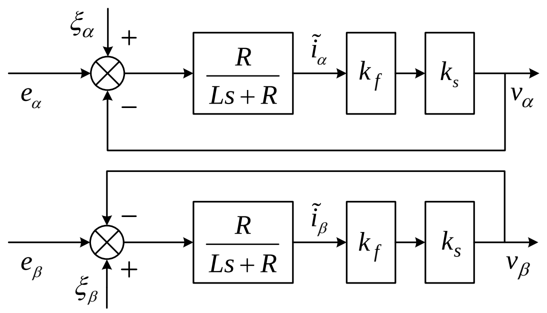

Fig. 3. Non-linear equivalent model of the SMO.

$$\Phi_{\text{SMO}}(s) = \frac{v_{\alpha,\beta}}{e_{\alpha,\beta}} = \frac{k_c}{\tau s + 1} \tag{13}$$

where $k_c = \frac{k_s k_f}{k_s k_f + 1}$, $\tau = \frac{L}{k_s k_f R + R}$. It is clear that the SMO has a low-pass characteristic that relies on k_f, k_s, R and L, which would lead to a phase lag to the position estimated. Through the non-linear equivalent model, the phase lag relating to the speed is

$$\theta_{ed} = -\arctan(\tau\omega_e) \tag{14}$$

Because k_f in θ_{ed} is unknown, the change law of k_f needs to be discussed to confirm the phase-frequency characteristic of the SMO. Fig. 4 shows the comparison of the sign and sigmoid functions according to (12). The essential difference between the two functions is that around zero, the sigmoid function is continuous while the sign function is discontinuous. Although the equivalent gains of the two functions tend to be consistent with the increase of the input, they are different when the input is small. After the initial reaching phase, states of the SMO slide along the sliding surface. Therefore, the properties of the switching functions around zero have a significant impact on the performance of the SMO.

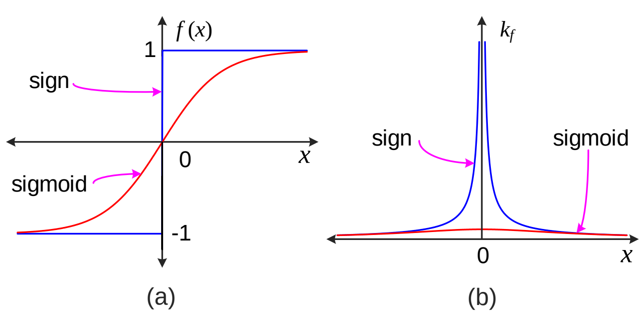

Fig. 4. Comparison of the sign and sigmoid functions. (a) Functions. (b) Equivalent gains.

Fig. 5 shows a simulation result of the equivalent gains of the sign and sigmoid functions when the SMO is on the sliding surface. When the sliding mode occurs, the input of the SMO fluctuates above and below zero. In this case, k_{fn} tends to be infinity while k_{fd} tends to be constant, which explains the reason why the sign function based SMO has a serious chattering problem while that of the sigmoid function has a considerable phase lag. Therefore, when the sigmoid function is adopted as the switching function, effective measures should be taken to compensate for the phase lag of the SMO. It can also be seen from Fig. 5 that the equivalent gain of the sigmoid function is smooth enough to calculate and compensate the phase lag according to (14).

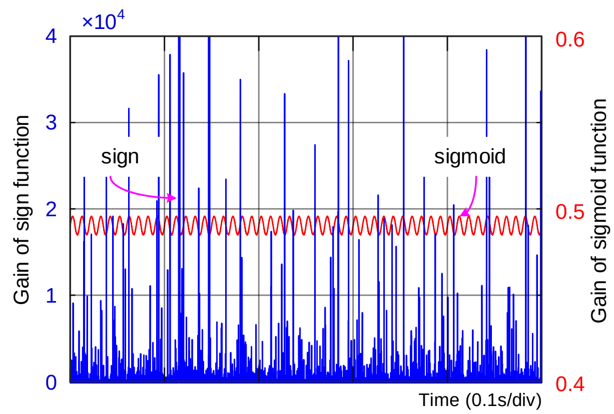

Fig. 5. Simulation result of the equivalent gains of the sign and sigmoid functions when the SMO is on the sliding surface.

B. Analysis of Conventional PLL

The conventional PLL has shown satisfactory performance in tracking the rotor position under a constant speed operation. However, it suffers from a serious position estimation error when the speed is non-constant. To investigate the reason, the following analyzes the characteristics of the conventional PLL. From Fig. 2, a back EMF error $\Delta E'$ is defined as

$$\begin{aligned}\Delta E' &= -\hat{e}_\alpha \cos\left(\hat{\theta}_e\right) - \hat{e}_\beta \sin\left(\hat{\theta}_e\right) \\ &= -k_L \sin(\Delta\theta_e)\end{aligned} \tag{15}$$

where $k_L = \psi_f \omega_e$, $\Delta\theta_e = \hat{\theta}_e - \theta_e$. When the PLL has tracked the rotor position, $\sin(\Delta\theta_e)$ is so small that $\sin(\Delta\theta_e)$ is approximately equal to $\Delta\theta_e$. From this, equation (15) can be rewritten as

$$\Delta E' \approx -k_L \Delta\theta_e \tag{16}$$

As shown in (16), k_L is a variable, and for ease of analysis and parameter tuning, $\Delta E'$ is normalized as

$$\Delta E \approx -\Delta\theta_e \tag{17}$$

Therefore, the equivalent diagram of the conventional PLL is shown in Fig. 6, and the open-loop transfer function of the conventional PLL $G_0(s)$ relating the output $\hat{\theta}_e$ to the input θ_e under a certain speed is

$$G_0(s) = \frac{\hat{\theta}_e(s)}{\theta_e(s)} = \frac{k_p s + k_i}{s^2} \tag{18}$$

It is well known that a step input in speed appears as a ramp input in position, and similarly, a ramp input in speed appears as a parabolic input in position. Thus, the conventional PLL can track the position ramp input with zero steady-state error since it is a type-II control system. However, when the motor accelerates or decelerates, the speed behaves as a ramp signal. Under such a circumstance, the conventional PLL is not fast

TABLE I
MOTOR PARAMETERS

Symbols	Parameters	Values
Pn	Number of pole pairs	4
J	Moment of inertia	0.003 kg·m2
R	Stator phase resistance	0.95 Ω
L	Stator phase inductance	12.5 mH
ψ_f	Flux linkage	0.183 Wb
T_e	Rated torque	5 N·m
n	Rated speed	1500 r/min
U_d	Rated voltage	311 V
I	Rated current	10 A

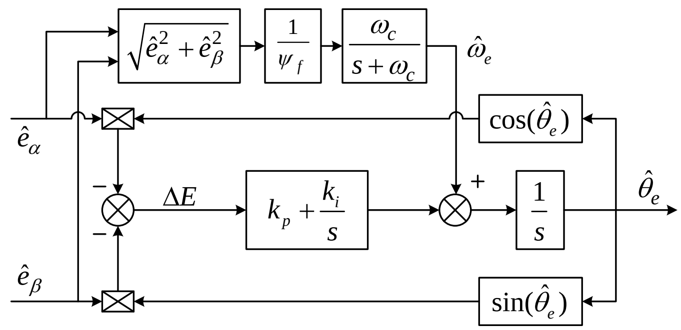

Fig. 7. Diagram of the proposed feed-forward PLL.

enough to track the position input with zero steady-state error. It is noted that the steady-error in the context refers to the steady-state position error.

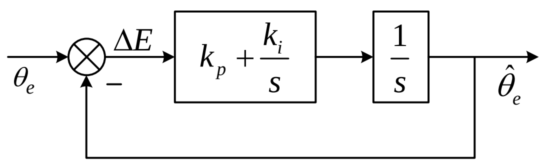

Fig. 6. Equivalent diagram of the conventional PLL.

To quantitatively analyze the steady-state error, an error transfer function of the conventional PLL is established as

$$\Phi_{er0}\left(s\right)=\frac{\Delta E\left(s\right)}{\theta_e\left(s\right)}=\frac{s^2}{s^2+k_ps+k_i} \tag{19}$$

Using the final value theorem, the steady-state error for a $\Delta\omega_e$ input is

$$\begin{aligned} e_{ss0} &= \lim_{s\to 0} s\Phi_{er0}\left(s\right)\frac{\Delta\omega_e}{s^3} \\ &= \frac{\Delta\omega_e}{k_i} \end{aligned} \tag{20}$$

It is clear from (20) that the position tracking error is proportional to the acceleration. Although increasing k_i can reduce the error, it is not a feasible method as the side effect is apparent. As shown in (15), because the input of the loop filter is similar to a sinusoidal wave, an excessive k_i would weaken the filter capacity and lead to unacceptable position harmonic error.

C. Design and Analysis of Proposed Feed-forward PLL

Since the steady-state tracking error cannot be eliminated by increasing k_i, this paper proposes an improved PLL by introducing a feed-forward path to the conventional PLL, as shown in Fig. 7, where a low pass filter is adopted to filter out the high-frequency noise and disturbance.

From Fig. 7, the open-loop transfer function of the proposed feed-forward PLL is

$$G_1\left(s\right)=\frac{\hat{\theta}_e\left(s\right)}{\theta_e\left(s\right)}=\frac{(k_p+\omega_c)s^2+(k_i+k_p\omega_c)s+k_i\omega_c}{s^2(s+\omega_c)} \tag{21}$$

where ω_c is the cut off frequency of the low pass filter in the feed-forward path. Accordingly, the closed-loop transfer function of the feed-forward PLL is

$$\Phi_1\left(s\right)=\frac{\hat{\theta}_e\left(s\right)}{\theta_e\left(s\right)}=\frac{(k_p+\omega_c)s^2+(k_i+k_p\omega_c)s+k_i\omega_c}{s^3+(k_p+\omega_c)s^2+(k_i+k_p\omega_c)s+k_i\omega_c} \tag{22}$$

To study the steady-state performance of the feed-forward PLL, its error transfer function is given by

$$\Phi_{er1}\left(s\right)=\frac{\Delta E\left(s\right)}{\theta_e\left(s\right)}=\frac{s^3}{(s+\omega_c)(s^2+k_ps+k_i)} \tag{23}$$

The Taylor series expansion of (23) with respect to s around the expansion point 0 is

$$\Phi_{er1}\left(s\right)=C_0+C_1s+C_2s^2+C_3s^3+C_4s^4+o\left(s^4\right) \tag{24}$$

where $C_0=0$, $C_1=0$, $C_2=0$, $C_3=\frac{1}{k_i\omega_c}$ and $C_4=-\frac{k_p}{k_i^2\omega_c}$; $o\left(s^4\right)$ is the high-order infinitesimal of s^4.

It is assumed that a parabolic position input of the feed-forward PLL is

$$\theta_e\left(t\right)=\frac{1}{2}\Delta\omega_et^2 \tag{25}$$

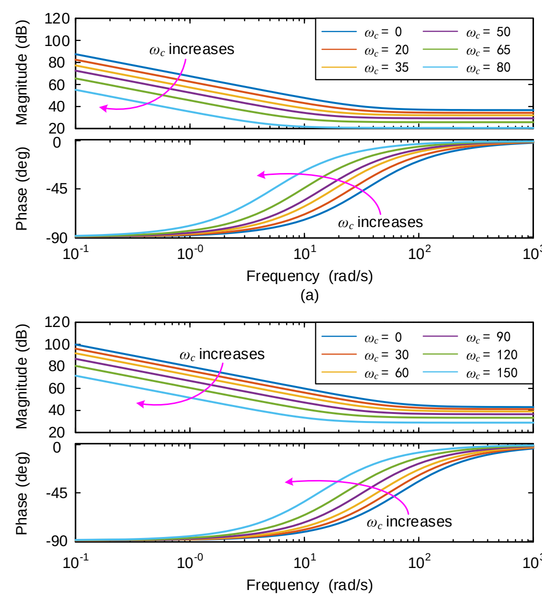

Fig. 8. Bode plots of the loop filters of the PLLs with different bandwidths. (a) Bandwidth = 100 rad/s. (b) Bandwidth = 200 rad/s.

This article has been accepted for publication in a future issue of this journal, but has not been fully edited. Content may change prior to final publication. Citation information: DOI 10.1109/JESTPE.2020.2967508, IEEE Journal of Emerging and Selected Topics in Power Electronics

and its time derivatives are

$$\begin{cases} \theta'_e(t) = \Delta\omega_e t \\ \theta''_e(t) = \Delta\omega_e \\ \theta'''_e(t) = 0 \end{cases} \tag{26}$$

Therefore, the steady-state tracking error of the feed-forward PLL for a speed ramp input is

$$\begin{aligned} e_{ss1}(t) &= C_0\theta_e(t) + C_1\theta'_e(t) + C_2\theta''_e(t) + C_3\theta'''_e(t) + \cdots \\ &= 0 \end{aligned} \tag{27}$$

It is clear from (27) that the feed-forward PLL can track a parabolic position input with zero steady-state tracking error. It also indicates that the feed-forward PLL can track a speed step and ramp inputs with zero steady-state tracking error.

The position harmonic error is related to the filtering capacity of the PLL that mainly depends on the loop filter. To compare the filtering performance of the conventional PLL with the proposed feed-forward PLL, Fig. 8 shows the Bode plots of the loop filters of the PLLs with different bandwidths. The bandwidths in Fig. 8 (a) and (b) are 100 rad/s and 200 rad/s, respectively.

It can be seen from Fig. 8 that the amplitude of the loop filter of the feed-forward PLL is smaller than that of the conventional PLL at full-frequency band, and with the increase of ω_c, the amplitude decreases. A lower amplitude, especially at a low-frequency band, is of great benefit to enhancing the filtering performance. Therefore, the feed-forward PLL can obtain a better position estimation performance in reducing the position harmonic error with the same bandwidth as the conventional PLL. It can also be seen from the two plots that with the increase of the bandwidth, the amplitude of the loop filter of the conventional PLL increases. However, even with higher bandwidth, the feed-forward PLL can also obtain a reasonable loop filter gain by tuning ω_c, which suggests that the feed-forward PLL can achieve a better harmonic suppression ability comparing to the conventional PLL.

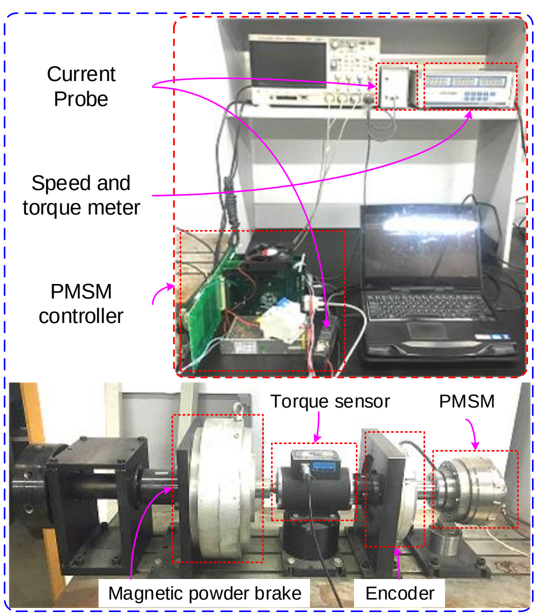

Fig. 9. Experimental platform.

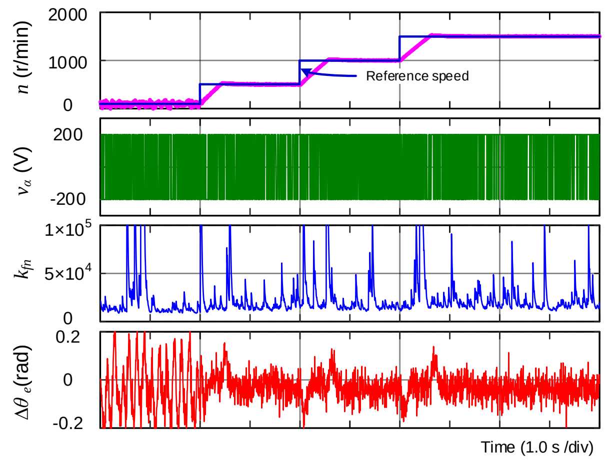

Fig. 10. Estimated speed, output of the SMO, equivalent gain and position estimation error when the sign function is adopted.

IV. Experimental Evaluation

To evaluate the performance of the proposed high-precision sensorless drive method of the PMSM, a field-oriented control platform is constructed, as shown in Fig. 9. The parameters of the prototype PMSM are listed in TABLE I. The field-oriented controller is based on a digital signal processor TMS320F28335. It is applied to execute the control algorithm, realize the detection of measurement signals, and generate the drive signals. The PMSM is driven by an IGBT based intelligent power module (IPM) PM50RL1A060 with a switching frequency of 10 kHz. A PI controller is used as the speed controller, where the proportional coefficient is 0.5, and the integral coefficient is 2.5. To limit the output of the speed

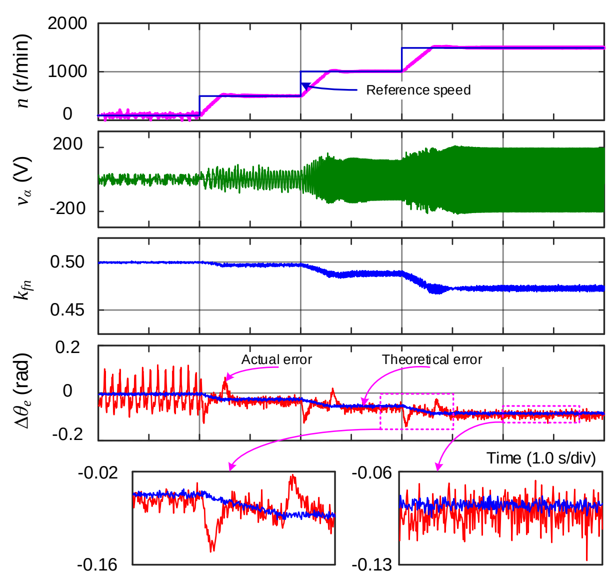

Fig. 11. Estimated speed, output of the SMO, equivalent gain and position estimation error when the sigmoid function is adopted.

This article has been accepted for publication in a future issue of this journal, but has not been fully edited. Content may change prior to final publication. Citation information: DOI 10.1109/JESTPE.2020.2967508, IEEE Journal of Emerging and Selected Topics in Power Electronics

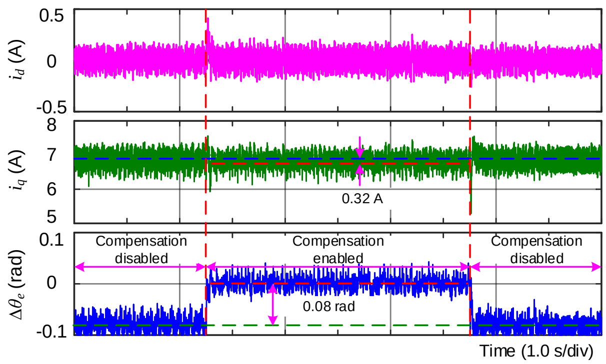

Fig. 12. d-q axis currents and position estimation error with and without the phase self-compensation method of the SMO.

controller, the upper and lower limits are set as 10 and -10, respectively.

A. Evaluation of Phase Self-compensation Method of SMO

To demonstrate the performance of the SMO with the sign and sigmoid function, Fig. 10 and Fig. 11 show the estimated speed n, the output of the SMO v_α, the equivalent gain k_{fn}, k_{fd}, and the position estimation error $\Delta\theta_e$. In order to verify the theoretical analysis of the phase lag characteristic of the SMO, the motor increases from 100 r/min to 1500 r/min. At 500 r/min, 1000 r/min and 1500 r/min, the motor keeps to a constant speed for a while.

As shown in Fig. 10, when the sign function is adopted, the equivalent gain k_{fn} always maintains a large value, and therefore, the position estimation deviation is small enough to be neglected. Moreover, because of the discrete output of the SMO and the irregular change of k_{fn}, the estimated position has a significant harmonic error. Therefore, due to the poor position estimation performance, the sign function based SMO is gradually replaced.

By contrast, the sigmoid function has a smaller equivalent gain than that of the sign function around zero. Replacing the sign function with the sigmoid function can effectively reduce the position harmonic error. As shown in Fig. 11, the estimated position also becomes smoother. However, it is observed from $\Delta\theta_e$ that there is a non-negligible position estimation deviation when the sigmoid function is adopted. When the motor operates at 1500 r/min, the position estimation deviation is up to 0.08 rad. As presented in (14), the phase lag is proportional to the speed in theory. As shown at the bottom sub-figure of Fig. 11, the position error increases with the increase of the speed, which is consistent with the theoretical value. Therefore, the position estimation deviation can be compensated through (14), which can eliminate the position estimation deviation caused by the phase lag of the SMO.

To evaluate the performance of the phase self-compensation method of the SMO, Fig. 12 shows the d-q axis currents and position estimation error with and without the phase self-compensation method. At 1.25s and 3.75s, the phase self-compensation method is enabled and disabled, respectively. It is clear that when the phase self-compensation method is enabled, the position estimation deviation is almost reduced to 0, and the q-axis current is also reduced by 0.32 A. Therefore, the phase self-compensation method can effectively compensate the phase lag caused by the SMO to improve the efficiency of the motor.

B. Evaluation of Feed-forward PLL

In this experiment, the error characteristic of the conventional PLL is verified, and the performance of the proposed feed-forward PLL is also demonstrated with different bandwidths.

Fig. 13 shows the position estimation error of the conventional PLL under acceleration and deceleration operations. It is clear from Fig. 13 that the conventional PLL can track the position with zero steady-state error whether at low speed or high speed. However, when the motor accelerates or decelerates, there is a steady-state position tracking error. Clearly, the error relating to the acceleration is too large to be neglected. With no load condition, the position estimation errors are up to 0.355 rad and 0.449 rad when the motor accelerates and decelerates, respectively. Moreover, when the motor decelerates with rated load condition, the error is up to 0.623 rad, which would lead to a risk of tracking failure. As analyzed in (20), the steady-state position error is proportional to $\Delta\omega_e$ and inversely proportional to k_i. In order to verify the analysis, the second plots in Fig. 13 (a) and (b) give the theoretical position error curves $\frac{\Delta\omega_e}{k_i}$. It is clear that the position tracking error is consistent with the theoretical value, which verified the correctness of the analysis of the conventional PLL.

As presented in (27), the proposed feed-forward PLL can track the position with zero steady-state error when the motor possesses acceleration. Fig. 14 and Fig. 15 show the position and speed estimation results with different bandwidths. It can be seen from Fig. 14 and Fig. 15 that all the conventional PLLs have a steady-state position tracking error when the motor accelerates or decelerates while the proposed feed-forward PLL can track the position without steady-state error.

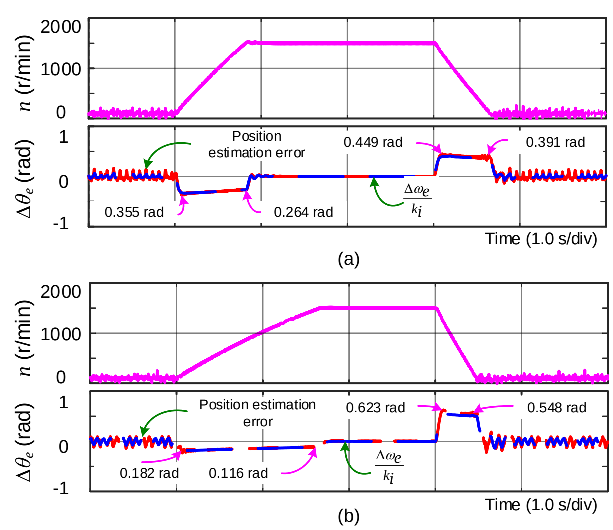

Fig. 13. Position estimation error of the conventional PLL under acceleration and deceleration operations. (a) With no load condition. (b) With rated load condition.

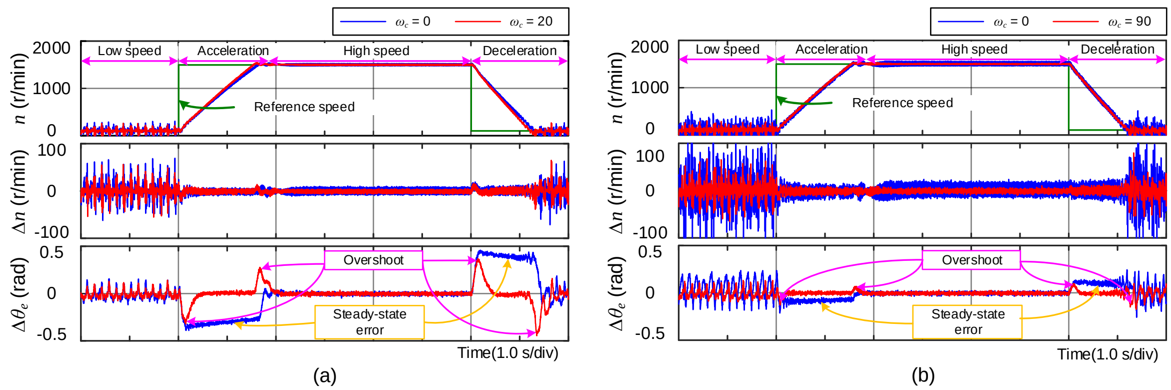

Fig. 14. Experimental comparison of the conventional and the proposed feed-forward PLL with different bandwidths for a speed step input of 100 – 1500 – 1000 r/min with no load condition. (a) Bandwidth = 100 rad/s. (b) Bandwidth = 200 rad/s.

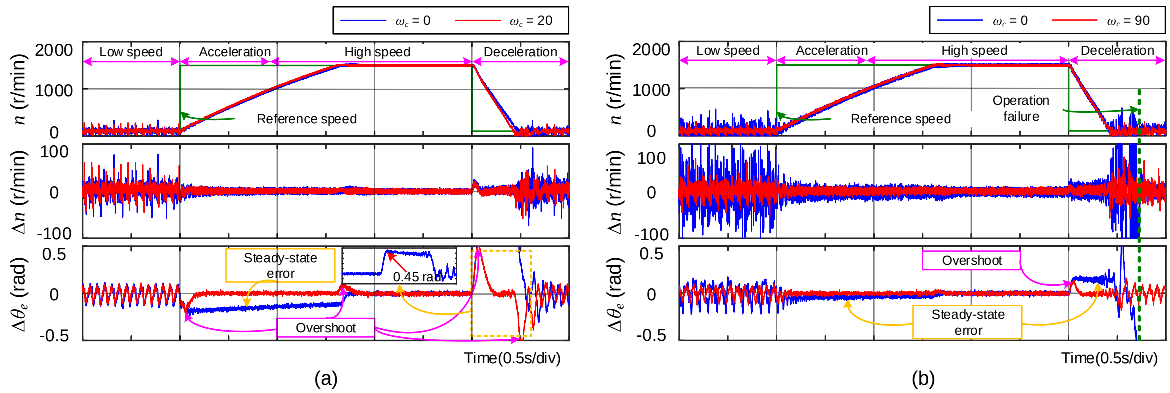

Fig. 15. Experimental comparison of the conventional and the proposed feed-forward PLL with different bandwidths for a speed step input of 100 – 1500 – 1000 r/min with rated load condition. (a) Bandwidth = 100 rad/s (b) Bandwidth = 200 rad/s.

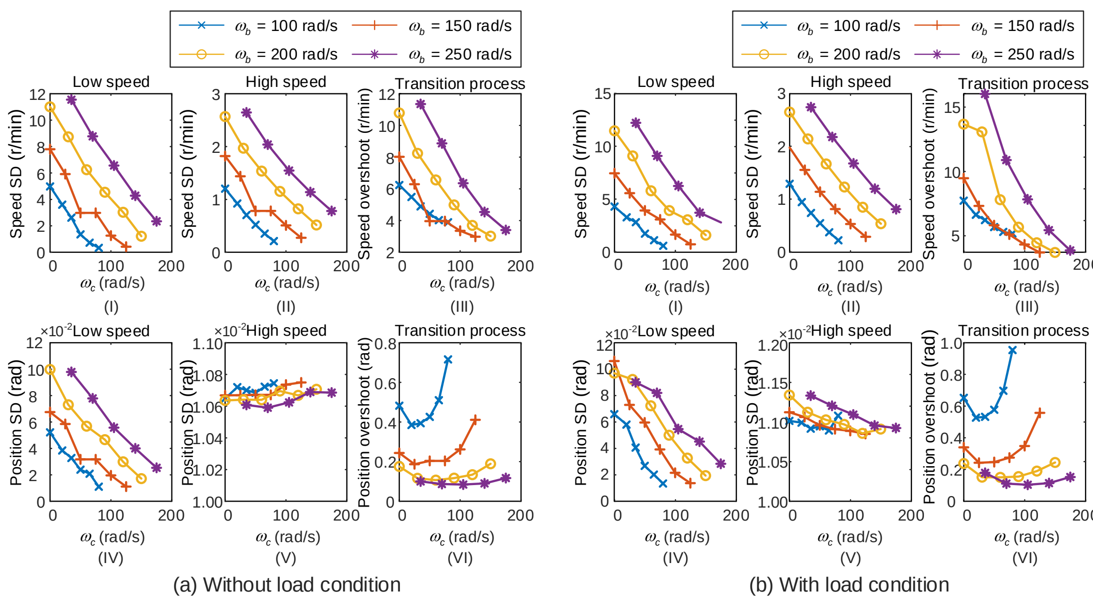

Fig. 16. Statistical analysis of the conventional and the proposed feed-forward PLLs with and without load condition. (I) Speed SD at 100 r/min. (II) Speed SD at 1500 r/min. (III) Overshoot of the speed estimation error in acceleration and deceleration. (IV) Position SD at 100 r/min. (V) Position SD at 1500 r/min. (VI) Overshoot of the position estimation error in acceleration and deceleration.

Since the steady-state position error of the conventional PLL is inversely proportional to k_i, and increasing k_i can reduce the steady-state error. However, an excessive k_i would lead to integral saturation and oscillation, which exposes the system to a risk of tracking failure. As shown in Fig. 15 (b), when k_i is excessive, the system has failed to operate. By contrast,

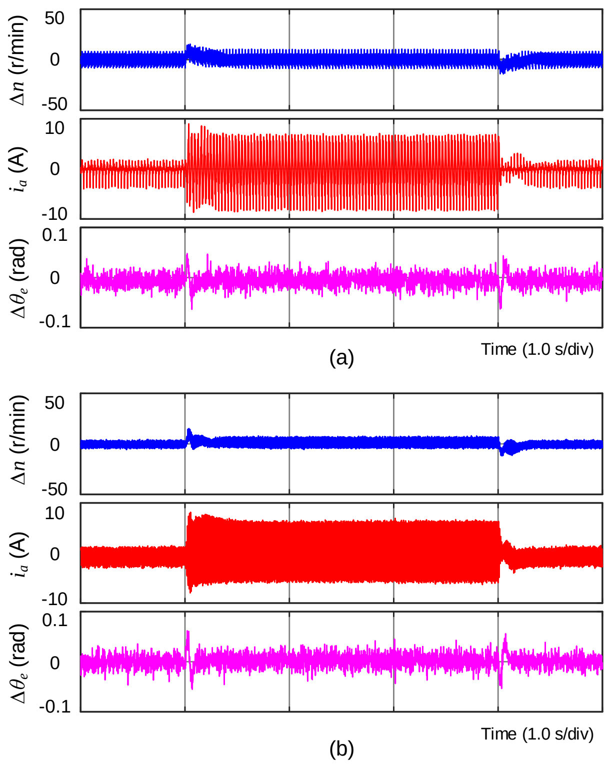

Fig. 17. Position estimation performance of the proposed feed-forward PLL with the step load disturbance. (a) 500 r/min. (b) 1500 r/min.

the proposed feed-forward PLL can track the position stably even with higher bandwidth.

According to Fig. 14 and Fig. 15, Fig. 16 gives the statistical analysis of the conventional and the proposed feed-forward PLLs. The standard deviation (SD) is introduced to quantify the amount of variations of the speed and position estimation. It has been noted that when $\omega_c = 0$, the feed-forward PLL degenerates into the conventional PLL. It is clear from Fig. 16 (I), (II), (IV) and (V) that the SDs of the position and speed are reduced with the increase of ω_c with or without load condition. It suggests that the proposed feed-forward PLL has a better performance in suppressing the position and speed harmonics, and a larger ω_c is of benefit to reducing the position and speed harmonic errors.

However, in the transition processes, as shown Fig. 16 (III) and (VI), the overshoots of the position estimation error relating to ω_c are not monotonic, and there exists an inflection point. Furthermore, with the increase of the bandwidth, the SDs of the speed and position would get worse. However, a smaller bandwidth would reduce the dynamic performance and lead to an excessive overshoot of the position estimation, which harms the stability of the system. Therefore, a reasonable parameter design of the bandwidth and ω_c can ensure a good performance of the feed-forward PLL.

Fig. 17 (a) and (b) show the position estimation performance of the proposed feed-forward PLL with the step load disturbance at 500 r/min and 1500 r/min, respectively. From top to bottom, the speed estimation error Δn, the current phase A i_a, and the position estimation error $\Delta\theta_e$ are given, respectively. As shown in Fig. 17, the related load is added at 1.0 s and removed at 4.0 s. It can be seen that adding and removing the load hardly affect the accuracy of rotor position estimation. It verified the effectiveness of the proposed feed-forward under the load changes at low and high speed.

V. Conclusion

Based on the analysis of the conventional sensorless drive method with the SMO and PLL, this paper proposed a position estimation deviation suppression technology combining the phase self-compensation SMO and the feed-forward PLL. Through the proposed non-linear equivalent model of the SMO, the position estimation deviation caused by the phase lag of the SMO is compensated in real-time. In variable speed applications, the conventional PLL shows a poor position estimation performance and suffers from a steady-state position estimation deviation under acceleration and deceleration operations. Contrary to increasing the bandwidth of the PLL, the feed-forward PLL has a smaller loop filter gain comparing to the conventional PLL, which is competent for eliminating the deviation and reducing the harmonic position error. A series of experiments verified the effectiveness of the proposed position estimation deviation suppression technology. It is noted that the proposed phase lag analysis method of the SMO provides a practical reference for analyzing the phase characteristics of other observers.

References

[1] J. Choi, K. Nam, A. A. Bobtsov, A. Pyrkin, and R. Ortega, "Robust adaptive sensorless control for permanent-magnet synchronous motors," *IEEE Transactions on Power Electronics*, vol. 32, no. 5, pp. 3989–3997, Jun. 2017.

[2] X. Song, B. Han, S. Zheng, and S. Chen, "A novel sensorless rotor position detection method for high-speed surface PM motors in a wide speed range," *IEEE Transactions on Power Electronics*, vol. 33, no. 8, pp. 7083–7093, Aug. 2018.

[3] H. Zhang and G. Liu, "Rotor position estimation method of permanent magnet synchronous motor with absolute position calculation and simple deviation compensation strategies," *Electronics Letters*, vol. 53, no. 25, pp. 1636–1637, 2017.

[4] M. S. Rafaq, F. Mwasilu, J. Kim, H. H. Choi, and J.-W. Jung, "Online parameter identification for model-based sensorless control of interior permanent magnet synchronous machine," *IEEE Transactions on Power Electronics*, vol. 32, no. 6, pp. 4631–4643, Jun. 2017.

[5] Z. Haifeng and L. Gang, "High-performance control method for the MSTMP motor," *IET Power Electronics*, dio:10.1049/iet-pel.2019.0488, in press, 2019.

[6] G. Wang, Z. Li, G. Zhang, Y. Yu, and D. Xu, "Quadrature PLL-based high-order sliding-mode observer for ipmsm sensorless control with online mtpa control strategy," *IEEE Transactions on Energy Conversion*, vol. 28, no. 1, pp. 214–224, Mar. 2013.

[7] X. Song, J. Fang, B. Han, and S. Zheng, "Adaptive compensation method for high-speed surface PMSM sensorless drives of emf-based position estimation error," *IEEE Transactions on Power Electronics*, vol. 31, no. 2, pp. 1438–1449, Feb. 2016.

[8] Y. Zhao, Z. Zhang, W. Qiao, and L. Wu, "An extended flux model-based rotor position estimator for sensorless control of salient-pole permanent-magnet synchronous machines," *IEEE Transactions on Power Electronics*, vol. 30, no. 8, pp. 4412–4422, Aug. 2015.

[9] W. Xu, Y. Jiang, C. Mu, and F. Blaabjerg, "Improved nonlinear flux observer-based second-order SOIFO for PMSM sensorless control," *IEEE Transactions on Power Electronics*, vol. 34, no. 1, pp. 565–579, Jan 2019.

[10] J. Solsona, M. I. Valla, and C. Muravchik, "A nonlinear reduced order observer for permanent magnet synchronous motors," *IEEE Transactions on Industrial Electronics*, vol. 43, no. 4, pp. 492–497, Aug. 1996.

[11] B. Hafez, A. S. Abdel-Khalik, A. M. Massoud, S. Ahmed, and R. D. Lorenz, "Single-sensor-based three-phase permanent-magnet synchronous motor drive system with luenberger observers for motor line

current reconstruction," *IEEE Transactions on Industry Applications*, vol. 50, no. 4, pp. 2602–2613, Jul. 2014.

[12] S. M. Gadoue, D. Giaouris, and J. W. Finch, "MRAS sensorless vector control of an induction motor using new sliding-mode and fuzzy-logic adaptation mechanisms," *IEEE Transactions on Energy Conversion*, vol. 25, no. 2, pp. 394–402, Jun. 2010.

[13] L. Sheng, W. Li, Y. Wang, M. Fan, and X. Yang, "Sensorless control of a shearer short-range cutting interior permanent magnet synchronous motor based on a new sliding mode observer," *IEEE Access*, vol. 5, pp. 18 439–18 450, Aug. 2017.

[14] T. Shi, Z. wang, and C. xia, "Speed measurement error suppression for PMSM control system using self-adaption kalman observer," *IEEE Transactions on Industrial Electronics*, vol. 62, no. 5, pp. 2753–2763, May 2015.

[15] D. Liang, J. Li, and R. Qu, "Sensorless control of permanent magnet synchronous machine based on second-order sliding-mode observer with online resistance estimation," *IEEE transactions on industry applications*, vol. 53, no. 4, pp. 3672–3682, Jul. 2017.

[16] Y. Feng, X. Yu, and F. Han, "High-order terminal sliding-mode observer for parameter estimation of a permanent-magnet synchronous motor," *IEEE Transactions on Industrial Electronics*, vol. 60, no. 10, pp. 4272–4280, Oct. 2013.

[17] S. Shao, P. W. Wheeler, J. C. Clare, and A. J. Watson, "Fault detection for modular multilevel converters based on sliding mode observer," *IEEE Transactions on Power Electronics*, vol. 28, no. 11, pp. 4867–4872, Nov. 2013.

[18] Y. Zhao, W. Qiao, and L. Wu, "An adaptive quasi-sliding-mode rotor position observer-based sensorless control for interior permanent magnet synchronous machines," *IEEE Transactions on Power Electronics*, vol. 28, no. 12, pp. 5618–5629, Dec. 2013.

[19] S.-C. Yang and G.-R. Chen, "High-speed position-sensorless drive of permanent-magnet machine using discrete-time EMF estimation," *IEEE Transactions on Industrial Electronics*, vol. 64, no. 6, pp. 4444–4453, Jun. 2017.

[20] Y. Zhao, W. Qiao, and L. Wu, "Improved rotor position and speed estimators for sensorless control of interior permanent-magnet synchronous machines," *IEEE Journal of Emerging and Selected Topics in Power Electronics*, vol. 2, no. 3, pp. 627–639, Dec. 2014.

[21] L. Zhao, J. Huang, H. Liu, B. Li, and W. Kong, "Second-order sliding-mode observer with online parameter identification for sensorless induction motor drives," *IEEE Transactions on Industrial Electronics*, vol. 61, no. 10, pp. 5280–5289, Oct. 2014.

[22] H. Kim, J. Son, and J. Lee, "A high-speed sliding-mode observer for the sensorless speed control of a PMSM," *IEEE Transactions on Industrial Electronics*, vol. 58, no. 9, pp. 4069–4077, Sept. 2011.

[23] S. Chi, Z. Zhang, and L. Xu, "Sliding-mode sensorless control of direct-drive PM synchronous motors for washing machine applications," *IEEE Transactions on Industry Applications*, vol. 45, no. 2, pp. 582–590, Mar. 2009.

[24] O. Saadaoui, A. Khlaief, M. Abassi, A. Chaari, and M. Boussak, "A sliding-mode observer for high-performance sensorless control of pmsm with initial rotor position detection," *International Journal of Control*, vol. 90, no. 2, pp. 393–408, May 2017.

[25] G. Wang, T. Li, G. Zhang, X. Gui, and D. Xu, "Position estimation error reduction using recursive-least-square adaptive filter for model-based sensorless interior permanent-magnet synchronous motor drives," *IEEE Transactions on Industrial Electronics*, vol. 61, no. 9, pp. 5115–5125, Sept. 2014.

[26] G. Wang, L. Ding, Z. Li, J. Xu, G. Zhang, H. Zhan, R. Ni, and D. Xu, "Enhanced position observer using second-order generalized integrator for sensorless interior permanent magnet synchronous motor drives," *IEEE Transactions on Energy Conversion*, vol. 29, no. 2, pp. 486–495, Jun. 2014.

[27] X. Dai, Z. Gao, T. Breikin, and H. Wang, "High-gain observer-based estimation of parameter variations with delay alignment," *IEEE Transactions on Automatic Control*, vol. 57, no. 3, pp. 726–732, Mar. 2011.

[28] Z. Gao, X. Dai, T. Breikin, and H. Wang, "Novel parameter identification by using a high-gain observer with application to a gas turbine engine," *IEEE Transactions on Industrial Informatics*, vol. 4, no. 4, pp. 271–279, Nov. 2008.

[29] Y. Kali, M. Ayala, J. Rodas, M. Saad, J. Doval-Gandoy, R. Gregor, and K. Benjelloun, "Current control of a six-phase induction machine drive based on discrete-time sliding mode with time delay estimation," *Energies*, vol. 12, no. 1, p. 170, Oct. 2019.

[30] Y. Kali, M. Saad, J. Doval-Gandoy, J. Rodas, and K. Benjelloun, "Discrete sliding mode control based on exponential reaching law and time delay estimation for an asymmetrical six-phase induction machine drive," *IET Electric Power Applications*, vol. 13, no. 11, pp. 1660–1671, 2019.

[31] G. Zhang, G. Wang, D. Xu, and N. Zhao, "Adaline-network-based PLL for position sensorless interior permanent magnet synchronous motor drives," *IEEE Transactions on Power Electronics*, vol. 31, no. 2, pp. 1450–1460, Feb. 2016.

[32] J. Lee, J. Hong, K. Nam, R. Ortega, L. Praly, and A. Astolfi, "Sensorless control of surface-mount permanent-magnet synchronous motors based on a nonlinear observer," *IEEE Transactions on Power Electronics*, vol. 25, no. 2, pp. 290–297, Feb. 2010.

[33] M. Abdelrahem, C. M. Hackl, and R. Kennel, "Finite position set-phase locked loop for sensorless control of direct-driven permanent-magnet synchronous generators," *IEEE Transactions on Power Electronics*, vol. 33, no. 4, pp. 3097–3105, Apr. 2017.

[34] M. Preindl and E. Schaltz, "Sensorless model predictive direct current control using novel second-order PLL observer for PMSM drive systems," *IEEE Transactions on Industrial Electronics*, vol. 58, no. 9, pp. 4087–4095, Sept. 2010.

[35] M. H. Bierhoff, "A general PLL-type algorithm for speed sensorless control of electrical drives," *IEEE Transactions on Industrial Electronics*, vol. 64, no. 12, pp. 9253–9260, Dec. 2017.

Gang Liu received the B.S. and M.S. degrees from Shandong University, Jinan, China, in 1992 and 1998, respectively, and the Ph.D. degree from Dalian University of Technology, Dalian, China, in 2001.

He is currently a Ph.D. Supervisor with the School of Instrumentation Science and Optoelectronics Engineering, Beihang University, Beijing, China. His research interests include spacecraft attitude control, high speed magnetically suspended motor and ultra-high sensitivity atomic magnetic field measurement.

Haifeng Zhang received the M.S. degree from Beihang University, Beijing, China, in 2016. He is currently working toward the Ph.D. degree at Beihang University, Beijing, China.

He is currently working toward the Ph.D. degree in precision instruments and machinery at the School of Instrumentation Science and Optoelectronics Engineering, Beihang University, Beijing, China. His research interests include permanent magnet motor control and power electronics.

Xinda Song received the B.S. degree in automation and M.S. degree in control theory and control engineering from Taiyuan University of Technology, Taiyuan, China, in 2004 and 2011, and the Ph.D. degree in precision instrument and machinery from the Beijing University of Aeronautics and Astronautics (BUAA), Beijing, China, in 2016. He was a Postdoctoral Research Fellow in the School of Instrumentation Science and Opto-electronics Engineering in BUAA.

He is currently with the Research Institute for Frontier Science, BUAA, where he is also a Research Member of the Key Laboratory of Fundamental Science for National Defense, Novel Inertial Instrument and Navigation System Technology. He obtained the 2018 Chinese Association of Automation excellent doctor degree dissertation award. His research interests include high-speed permanent magnet motor control and power electronics.